Alpine Precipitation Mechanisms in MAP IOP2b and 8

Robert A. Houze and Socorro Medina, University of Washington, Seattle, WA 98195, USA

1. Introduction

One of the primary strategies of the Mesoscale Alpine Programme (MAP, Bougeault et al. 2001) was to document the airflow and microphysics leading to heavy rainfall events in the Lago Maggiore region of northern Italy. Two particularly interesting cases of heavy rain in this region were the MAP Intensive Observation Periods IOP2b and IOP8. Each of these IOPs was associated with a strong 500-mb trough and strong southeasterly flow at the 850-mb level. Despite this large-scale similarity, the precipitation processes differed markedly between the two cases. In this study, we use data from the NCAR S-Pol polarimetric Doppler radar and output from the MAP operational runs of the Canadian Mesoscale Compressible Community Model (MC2, Benoit et al. 1997) to investigate these differences.

2. Polarimetric Doppler Radar Observations

The figures in this paper represent the airflow, precipitation, and microphysics in a vertical cross section extending southeast to northwest from the S-Pol radar northwestward up to the summit of the Alps. This section lies roughly parallel to the flow at the 2-km level. All the figures are mean or composite patterns. Figures 1a, c, and e contain data from the S-Pol radar for IOP2b, for 1500-1900 UTC 20 September. Figures 1b, d, and f contain data from the S-Pol radar for IOP8, for 0810-0850 UTC 21 October 1999. Cross sections averaged over the whole storm are qualitatively similar but less amplified. Figure 2 contains fields obtained by averaging hourly output from the MC2 over the time period of each IOP.

The mean reflectivity field (Fig. 1a) shows a well-defined convective echo structure (maximum echo > 40 dBZ) over the first peak of the mountain range, where the horizontal gradient of elevation first becomes very large. Smaller and weaker convective echo maxima appear just upwind of the major cell over the terrain. Steiner et al. (2000) noted two types of echoes in this storm: cells forming just upwind of and moving toward the mountains, and cells that were anchored to the terrain. The major maximum over the first peak of the range is the cumulative effect of the latter type of cell, while the small weaker average cellular structures just upwind were produced by the transient propagating cells that were not tied closely to the terrain.

The low-level maximum of reflectivity in the primary convective core tied to the first major mountain peak suggests that coalescence may have been important in the orographic enhancement of the convective precipitation forming over the peak of the terrain.

During IOP2b, particle-identification algorithms (Vivekanandan et al. 1999) were applied to S-Pol dual-polarization radar data. The outputs of the algorithm were accumulated over the 4-h time period of the cross sections in Fig. 1. The contours in Fig. 1c surround the regions of maximum occurrence of three types of ice particles: graupel, wet snow, and dry snow. The solid contours indicate that graupel occurred preferentially above the first major mountain peak, directly above the reflectivity maximum. Dry snow (long-dashed contours) surrounded the graupel. The small region of wet snow identified by the polarimetric data (dotted contours) evidently was the melting graupel—the maximum of graupel occurrence was above this line, while the reflectivity maximum lay just below. The maximum of graupel occurrence directly over the precipitation maximum seen in the reflectivity suggests that riming of ice particles just above the 0°C level and their subsequent fallout and melting may have been another major factor contributing to the reflectivity maximum at lower levels. The data in Figs. 1a and c thus suggest that both riming and coalescence played an important role in producing high precipitation accumulations over the lower windward portion of the Alps during IOP2b.

The radial velocity pattern in IOP2b (Fig. 1e) is consistent with the riming being produced by strong wind up and over the windward slope. The radial velocity data show that the graupel concentration was located over the first major peak in the topography at the downwind end of a radial velocity jet directed toward, up, and over the terrain. Evidently a low-level jet flowed to the mountains from the Po Valley and rose over the terrain when the airflow encountered the first major peak. This jet of Mediterranean air transported moisture above the 0°C level. This mechanism evidently saturated and condensed cloud liquid water, which was collected by raindrops below the 0°C level and accreted by ice particles above the freezing level. The accretion by ice particles of supercooled cloud liquid water condensed and transported by the jet up the terrain evidently led to the maximum of graupel occurrence seen in Fig. 1c. Simple parameterized microphysics in a rising parcel predict a maximum of rimed ice particle mass at about this altitude (Yuter and Houze 2001).

In contrast to IOP2b, the precipitation in IOP8 had a stratiform structure. The echo (Fig. 1b) was weaker (maximum ~34 dBZ), and a distinct bright band at the 2-km level extended upstream of the Alpine range. The particle identification during IOP8 (Fig. 1d) also exhibited a horizontally layered structure, characterized by wet snow in the

melting layer with dry snow above. The S-Pol radar detected no evidence of graupel whatsoever in this case. The radial velocity structure in IOP8 (Fig. 1f) contained an elevated jet around 3 km but it did not slope upward, and thus did not indicate any vertical motion at low levels, as was the case in IOP2b (cf. Fig. 1e). At low levels the radial component of the flow was toward the radar, indicating a return or blocked flow over the Po Valley (Bousquet and Smull 2001; Smull et al. 2001).

3. Model Airflow and Microphysics

The MC2 microphysical parameterization predicted four cloud hydrometeor types: cloud water, rain water, ice crystals, and graupel (Benoit et al. 1997, 2001; Kong and Yau 1997). Figure 2 shows model output for the same vertical cross section as Fig. 1, but with the MC2 topography. The microphysical particles predicted by the model over a time interval extending throughout IOP2b are shown in Fig. 2a. The average rain mixing ratio (short dashed contours) for this IOP was maximum over the middle mountain peak. The graupel (solid contours) and ice crystal (long dashed contours) mixing ratios were also greatest over the middle mountain peak. The model thus shows the most robust orographic precipitation process over the middle mountain peak. This predicted behavior differs from the actual rainfall, for which the radar data showed the maximum reflectivity and maximum graupel over the first (rightmost) mountain peak encountered by the windward flow (Figs. 1a and c). The model produced lesser maxima of rain over the first and third peaks. The maximum occurrence of graupel upwind of the first peak in Fig. 2a was evidently associated with the mobile convective cells that were not anchored to the topography and produced the weaker cells just upwind of the terrain in Fig. 1a. The more highly coherent and stronger maxima of microphysical variables over the middle peak were associated with the persistent flow over the topography throughout the IOP.

Using the model components of the velocity, the model radial velocity fields (i.e., the wind component that would have been seen by S-Pol) were constructed to compare with observations. The model radial velocity field for IOP2b (Fig. 2c) shows a low-level jet sloping up the terrain, reminiscent of the upslope radial velocity jet seen in the radar data. However, the model's version of the jet does not rise as abruptly as the real radial velocity maximum (cf. Fig. 1e), and it is stronger. The model topography has a 3-km resolution, which smoothes the topography. The heights of the three major peaks in the model cross section (Fig. 2) are therefore much lower than the real topography (Fig. 1). The radial velocity jet does not rise above the 3-km level in the model until the second peak (Fig. 2e), whereas in the real atmosphere the radial jet must rise above 3 km at the first major peak encountered by the jet (Fig. 1e). The vertical velocity maximum in the model is correspondingly associated with the second peak (Fig. 2e), and the production of graupel and rain are located there instead of over the first peak, as shown by the radar data (Figs. 1a and c). Evidently smoothing the topography can lead to prediction of heavy rain over the wrong peak of topography.

The MC2 mean microphysical fields over the whole period of IOP8 are shown in Fig. 2b. The 0°C level implied by the changeover from ice to rain at ~2.5 km is in agreement with the observed melting layer (Figs. 1b and d). The model, however, departs strongly from the observations by predicting the occurrence of graupel over the windward slope of the lowest peak of the terrain. As noted above, no graupel was detected in the polarimetric radar data during this storm. The calculated radial velocity for IOP8 (Fig. 2e) does predict an approximately horizontal jet at 3 km (i.e., not sloping with the terrain) with the observed magnitude. However, it does not capture the return flow at low levels. Both the lack of blocking at low levels and the prediction of graupel are probably the result of the MC2 not predicting the strong static stability that occurred at low levels in IOP8 (Houze et al. 2000).

4. Conclusions

The S-Pol radar observations in IOP2b suggest that coalescence played a role in the orographic convective precipitation maximum. The polarimetric data indicate a maximum frequency of occurrence of graupel just above the reflectivity maximum, suggesting that riming, fallout, and melting of ice particles at the top point of the rise of the radial velocity jet also contributed to the reflectivity rain maximum at lower levels. The MC2 predicted this behavior of the airflow and microphysics, but apparently because of smoothing of the topography, the MC2 predicted this behavior over the second terrain peak encountered by the radial flow rather than the first peak.

In IOP8, the S-Pol showed a horizontal jet of radial velocity at the 3-km level across the terrain of the Alps. At low levels the radial velocity was directed back toward the radar in association with the blocking that occurred in this storm. The polarimetric observations indicated no graupel formation at any time during the storm, only dry snow aloft with wet snow in a well-defined melting layer. The MC2 on the other hand did not show the blocked flow, and it predicted graupel formation just upwind of the first peak of the terrain. Both of these results probably stem from the MC2 not predicting the strong static stability at low levels.

References

Benoit, R., and Coauthors, 2001: The real-time ultrafinescale forecast support during the Special Observing Period of the MAP. *Bull. Amer. Meteor. Soc.,* submitted.

Benoit, R., and Coauthors, 1997: The Canadian MC2: A semi-Lagrangian, semi-implicit wide-band atmospheric model suited for finescale process studies and simulation. *Mon. Wea. Rev.,* **125,** 2382-2415.

Bougeault, P., and Coauthors, 2001: The MAP Special Observing Period. *Bull. Amer. Meteor. Soc.,* **82,** 433–462.

Bousquet, O., and B. Smull, 2001: Comparative study of two orographic precipitation events exhibiting significant upstream blocking during MAP. MAP Conf., Schliersee, Germany.

Houze, R. A., Jr., S. Medina, and M. Steiner, 2000: Two cases of heavy rain on the Mediterranean side of the Alps in MAP. Preprints, *9th Conf. on Mt. Meteor.,* Aspen, CO, Amer. Meteor. Soc., 1-5.

Kong F., and M. K. Yau, 1997: An explicit approach to microphysics in MC2. *Atmos.-Ocean,* **35,** 257-291.

Smull, B., O. Bousquet, and D. Lüthi, 2001: Evaluation of real-time MC2 simulation results for a case of significant upstream blocking during MAP. MAP Conf., Schliersee, Germany.

Steiner, M., and Coauthors, 2001: Space-time analysis of rainfall in relation to topography for heavy precipitation events observed during MAP. Preprints, *Ninth Conf. on Mt. Meteor.*, Aspen, CO, Amer. Meteor. Soc., 151-154.

Vivekanandan, J., and Coauthors, 1999: Cloud microphysics retrieval using S-band polarization radar measurements. *Bull. Amer. Meteor. Soc.,* **80,** 381-388.

Yuter, S. E., and R. A. Houze, Jr., 2001: Microphysical modes of precipitation growth determined by vertically pointing radar at Locarno-Monti during MAP. MAP Conf., Schliersee, Germany.

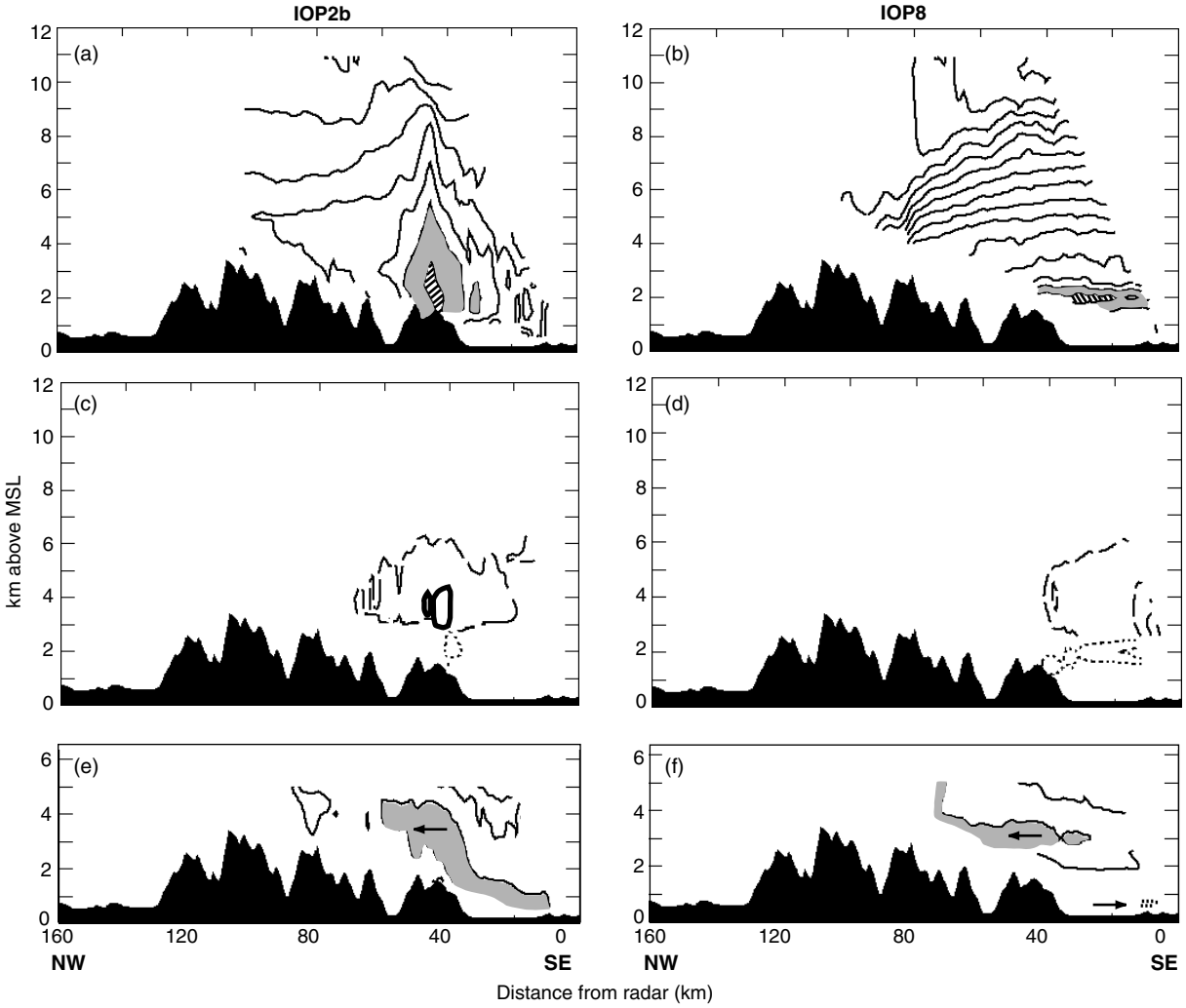

Figure 1. Southeast-northwest vertical cross section of S-Pol radar data. The section extends 160 km from the S-Pol radar, which was located at the southeast end of the cross section. The fields in the cross section panels have been either accumulated or averaged over 1500-1900 UTC 20 September 1999 for IOP2b and 0810-0850 UTC 21 October 1999 for IOP8. (a)-(b) Mean reflectivity. IOP2b—contours every 10 dB*Z*, dB*Z* = 32-42 shaded, dB*Z* > 42 hatched. IOP8—contours every 4 dB*Z*, dB*Z* = 30.5-34.5 shaded, dB*Z* > 34.5 hatched. (c)-(d) Particle types identified by polarimetric radar algorithms. Contours enclose regions of most frequent occurrence of dry snow (long-dashed: IOP2b, 30 counts; IOP8, 35, 235, and 435 counts), wet snow (short-dashed: IOP2b, 17 counts; IOP8, 29 and 129 counts), and graupel (solid: IOP2b, 20 counts). (e)-(f) Mean radial velocity. IOP2b— > 12 m s^{-1} shaded; IOP8— > 19.5 m s^{-1} shaded. Negative contour shown: -0.5, -3 m s^{-1}. Solid contours indicate flow towards the radar; dashed contours indicate flow away from the radar. Arrows indicate direction of horizontal component of radial velocity.

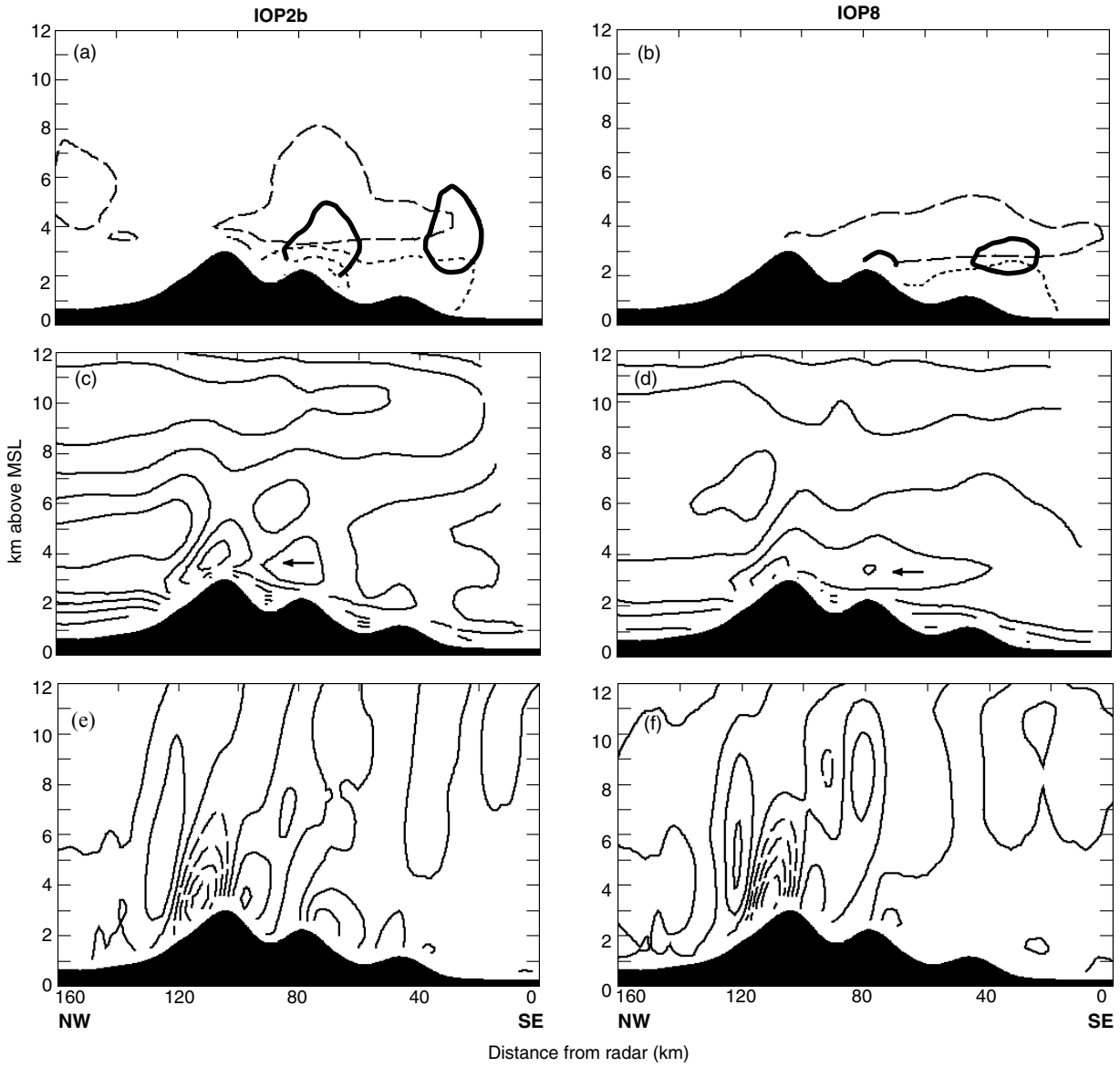

Figure 2. Southeast-northwest vertical cross section of MC2 model output for same cross section shown in Fig. 1. The fields in the cross section panels have been averaged from hourly model output to give average fields for IOP2b (1300 UTC 19 September through 0000 UTC 21 September 1999) and IOP8 (1200 UTC 20 October through 2200 UTC 21 October 1999). (a)-(b) Mean mixing ratios of ice (long-dashed contours: 2×10^3 contour shown), rainwater (short-dashed: IOP2b—contours every 1.3×10^4, maximum contour shown= 3.6×10^4; IOP8—1×10^4 contour shown), and graupel (solid: 1×10^5 contour shown). (c)-(d) Mean radial velocity from S-Pol radar location. IOP2b—contours every 3 m s^{-1}, maximum contour shown = 22 m s^{-1}). IOP8—contours every 5 m s^{-1}, maximum contour shown = 20 m s^{-1}. Arrows indicate direction of horizontal component of radial velocity. (e)-(f) Mean vertical velocity. Contours every 0.5 m s^{-1}, maximum contour shown = 1 m s^{-1}, minimum contour shown= -2 m s^{-1}. Solid contours indicate positive velocities; dashed contours indicate negative velocities.